

# Effect of the 2022 summer drought across forest types in Europe

Mana Gharun<sup>1</sup>, Ankit Shekhar<sup>2,3</sup>, Jingfeng Xiao<sup>4</sup>, Xing Li<sup>5</sup>, Nina Buchmann<sup>2</sup>

<sup>1</sup> Institute of Landscape Ecology, University of Münster, Münster, Germany

<sup>2</sup> Institute of Agricultural Sciences, ETH Zürich, Zürich, Switzerland

<sup>3</sup> Agricultural and Food Engineering Department, Indian Institute of Technology Kharagpur, Kharagpur, India

<sup>4</sup> Earth Systems Research Center, University of New Hampshire, New Hampshire, USA

<sup>5</sup> Research Institute of Agriculture and Life Sciences, Seoul National University, Seoul, South Korea

Correspondence to: Mana Gharun, mana.gharun@uni-muenster.de

## Abstract

Forests in Europe experienced record-breaking dry conditions during the 2022 summer. The direction in which various forest types respond to climate extremes during their growing season is contingent upon an array of internal and external factors. These factors include the extent and severity of the extreme conditions and the tree ecophysiological characteristics adapted to environmental cues, which exhibit significant regional variations. In this study we aimed to: 1) quantify the extent and severity of the extreme soil and atmospheric dryness in 2022 in comparison to two most extreme years in the past (2003 and 2018), 2) quantify response of different forest types to atmospheric and soil dryness in terms of canopy browning and photosynthesis, and 3) relate the functional characteristics of the forests to the emerging responses observed remotely at the canopy level. For this purpose, we used spatial meteorological datasets between 2000 to 2022 to identify conditions with extreme soil and atmospheric dryness. We used the near-infrared reflectance of vegetation (NIRv) derived from the MOderate Resolution Imaging Spectroradiometer (MODIS), and the Global OCO-2 Solar Induced Fluorescence (GOSIF) as an observational proxy for ecosystem gross productivity, to quantify the response of forests at the canopy level.

30 In summer 2022, southern regions of Europe experienced exceptionally pronounced  
31 atmospheric and soil dryness. These extreme conditions resulted in a 30% more  
32 widespread decline in GOSIF across forests compared to the drought of 2018, and 60%  
33 more widespread decline compared to the drought of 2003. Although the atmospheric  
34 and soil drought were more extensive and severe (indicated by a larger observed  
35 maximum z-score) in 2018 compared to 2022, the negative impact on forests, as  
36 indicated by declined GOSIF, was significantly larger in 2022. Different forest types were  
37 affected in varying degrees by the extreme conditions in 2022. Deciduous broad-leaved  
38 forests were the most negatively impacted due to the extent and severity of the drought  
39 within their distribution range. In contrast, areas dominated by Evergreen Needle-Leaf  
40 Forests (ENF) in northern Europe experienced a positive soil moisture (SM) anomaly and  
41 minimal negative vapor pressure deficit (VPD) in 2022. These conditions led to enhanced  
42 canopy greening and stronger solar-induced fluorescence (SIF) signals, benefiting from  
43 the warming. The higher degree of canopy damage in 2022, despite less extreme  
44 conditions, highlights the evident vulnerability of European forests to future droughts.

45

46 *Keywords: photosynthesis, soil drought, atmospheric drought, canopy browning, gross*  
47 *primary production*

## 48 **Introduction**

49 The frequency and intensity of drought events have been rising globally, and future global  
50 warming is expected to further increase their occurrence (Seneviratne et al. 2021;  
51 Röthlisberger and Papritz 2023). Particularly over the past two decades, many regions in  
52 Europe have experienced widespread drought conditions, notably during the summers of  
53 2003, 2010, and 2018 (Bastos et al. 2020; Zhou et al. 2023). The extreme conditions  
54 caused widespread ecological disturbances (Müller and Bahn 2022) and reduced the  
55 capacity of forests for carbon uptake, thereby diminishing their potential for mitigating  
56 climate change (van der Woude et al. 2023). Additionally, heatwaves and prolonged  
57 droughts stress vegetation, making it more susceptible to other biotic and abiotic stress  
58 factors. This increased vulnerability leads to higher tree mortality, elevated wildfire risks,

59 and a loss of biodiversity among plants and animals living at the edge of their temperature  
60 tolerance. These conditions also alter phenology and plant development, causing  
61 cascading effects on ecosystem functioning (Seidl et al. 2017).

62 The spatial extent and severity of drought events vary, and their impacts depend on local  
63 ecological characteristics of the forests, species-specific temperature and moisture  
64 thresholds that limit tree functioning, as well as adaptation strategies and acclimation of  
65 trees to more frequent and intense extreme conditions (Gessler et al. 2020). For example,  
66 comparing the 2003 and 2018 extreme years, the year 2018 was characterized by a  
67 climatic dipole, featuring extremely hot and dry weather conditions north of the Alps but  
68 comparably cool and moist conditions across large parts of the Mediterranean. Negative  
69 drought impacts appeared to affect an area 1.5 times larger and to be significantly  
70 stronger in summer 2018 compared to summer 2003 (Buras et al. 2020).

71 In 2022, Europe faced its second hottest and driest year on record, with the summer of  
72 that year being the warmest summer ever recorded. Conditions in summer 2022 led to  
73 record-breaking heatwave and drought events across many regions (Copernicus Climate  
74 Change Service, 2023). Compound drought and heatwave conditions in 2022 caused  
75 widespread crop damage, water shortages, and wildfires across Europe. The hardest-hit  
76 areas were the Iberian Peninsula, France, and Italy, where temperatures exceeded 2.5°C  
77 above normal, and severe droughts persisted from May to August (Tripathy and Mishra  
78 2023). The reduced soil moisture due to precipitation deficits and high temperatures,  
79 contributed to the persistence and severity of drought, creating a positive feedback loop  
80 where dry soils led to even drier conditions (Tripathy and Mishra 2023).

81 Drought and heatwaves have a range of detrimental effects on trees and forests. The  
82 most immediate impact is that elevated air temperatures and increased dryness, whether  
83 in the soil or in the atmosphere, disrupt mesophyll and stomatal conductance, thereby  
84 impairing carbon uptake (Marchin et al. 2022). Plants reduce stomatal conductance under  
85 severe drought to reduce water stress at the expense of reduced rates of photosynthesis  
86 (Oren et al., 1999). Drought also increases the chance of hydraulic failure, which can lead  
87 to tree mortality (Choat et al. 2018). Additionally, rising temperatures reduce the  
88 enzymatic activity in trees, which in turn diminishes the forest's gross primary productivity  
89 (Gourlez de la Motte et al. 2020). Elevated temperatures can also increase respiration

90 rates in both soil and trees, which reduces the forest's net carbon uptake and their ability  
91 to mitigate anthropogenic CO<sub>2</sub> emissions (van der Molen et al. 2011; Anjileli et al. 2021).  
92 Drought also restricts the movement of nutrients in soil water, reducing their availability  
93 to trees and consequently impacting their growth and productivity (Bauke et al. 2022).  
94 Changes in plant water-use and nutrient cycling can trigger feedback loops that magnify  
95 the effects of drought and heat stress. For instance, reduced plant cover can increase  
96 soil temperatures and further accelerate water loss and increase plant water demand  
97 (Haesen et al. 2023). On the other hand, increased atmospheric dryness or reduced soil  
98 moisture levels increase stomatal closure which limits transpiration and leads to higher  
99 leaf temperature that intensifies heat stress on plants (Drake et al. 2018). Reduced  
100 transpiration and photosynthesis elevate surface temperatures and atmospheric CO<sub>2</sub>  
101 concentrations, altering local and regional climate patterns and intensifying the frequency  
102 and severity of extreme events (Humphrey et al. 2018). These effects vary significantly  
103 depending on forest type and species composition. Together with the characteristics of  
104 the extreme events themselves – such as their extent and severity- this variability  
105 complicates our understanding of how drought affects the functionality of different forest  
106 ecosystems (Gharun et al. 2020; Shekhar et al. 2023). These feedback loops highlight  
107 the urgent need to assess how climate extremes impact different forest types, which are  
108 crucial for sequestering significant portions of anthropogenic emissions. Our study aims  
109 to 1) quantify the extent and severity of the extreme conditions in 2022 – focusing on soil  
110 and atmospheric dryness- and compare them to those of two previous extreme years  
111 (2003, 2018), 2) quantify the responses of different forest types to drought in terms of  
112 canopy browning and photosynthesis, and 3) connect the functional characteristics of the  
113 forests with the canopy-level responses observed.

## 114 **Methods**

### 115 *Meteorological dataset*

116 We used Europe-wide gridded datasets covering daily mean air temperature (T<sub>air</sub>; °C),  
117 daily mean relative humidity (RH; %) and daily mean soil moisture (SM; m<sup>3</sup>m<sup>-3</sup>) for the  
118 topsoil layer (0-7 cm depth), spanning from 2000-2022. The study area encompasses

119 longitudes from 11°W to 32°E, and latitudes from 35.8°N to 72°N, approximately 4.45  
120 million km<sup>2</sup>. We sourced the Tair and RH datasets from the E-OBS v27.0e dataset which  
121 provides daily data at 0.1°×0.1° spatial resolution (Cornes et al., 2018; Klein et al., 2002).  
122 We calculated daily mean vapor pressure deficit (VPD; kPa) from Tair and RH using  
123 Equation 1 (Dee et al. 2011).

124

$$125 \quad VPD = \left(1 - \frac{RH}{100}\right) \times 0.6107 \times 10^{\frac{7.5 \times T_{air}}{237.3 + T_{air}}} \quad (1)$$

126

127 The topsoil SM dataset was extracted from the most recent reanalysis data from  
128 ECMWF's (European Centre for Medium-range Weather Forecasts) new land component  
129 of the fifth generation of European Reanalysis (ERA5-Land) dataset (daily at 0.1°×0.1°  
130 resolution; Munoz-Sabater et al., 2021). ERA5-Land provides soil moisture (SM) data at  
131 an hourly interval with a spatial resolution of 0.1° × 0.1°. For our analysis, we aggregated  
132 the hourly SM data into daily averages. Recent validation studies using in-situ  
133 measurements and satellite data have confirmed the high accuracy of surface SM  
134 simulations from ERA5-Land (Albergel et al., 2012; Lal et al., 2022; Muñoz-Sabater et al.,  
135 2021). Additionally, SM data from ERA5-Land have been utilized to investigate drought  
136 and global SM patterns (see Lal et al., 2023; Shekhar et al., 2024b). We re-sampled the  
137 Tair, VPD, and SM data from daily (0.1° × 0.1°) to 8-day (0.05° × 0.05°) intervals to align  
138 with the temporal and spatial resolution of the vegetation response dataset (see below).

### 139 *Forest canopy response dataset*

140 In order to assess the forest canopy response to drought stress, we used two satellite-  
141 based proxies:

142 1) The structure-based NIRv (Near-Infrared Reflectance of Vegetation) index derived  
143 from MODIS (Moderate Resolution Imaging Spectroradiometer; 8-day 500m x 500m  
144 MOD09Q1 v6.1 product) which is calculated using surface spectral reflectance at near-  
145 infrared band ( $R_{NIR}$ ) and red band ( $R_{Red}$ ) as shown in Equation 2 (Badgley et al. 2017).  
146 The calculated NIRv at 500m resolution was aggregated to a 0.05°×0.05° resolution  
147 (daily) by averaging.

148

$$149 \quad NIR_V = R_{NIR} \times \frac{R_{NIR} - R_{Red}}{R_{NIR} + R_{Red}} \quad (2)$$

150

151 2) The physiological-based reconstructed global OCO-2 (Observation Carbon  
152 Observatory - 2) solar induced fluorescence (GOSIF) dataset. Solar-induced  
153 fluorescence (SIF) is an energy flux (unit:  $Wm^{-2}\mu m.sr^{-1}$ ) re-emitted as fluorescence by the  
154 chlorophyll *a* molecules in the plants during photosynthesis (Baker, 2008). Recent  
155 extensive research has established a strong link between Solar-Induced Fluorescence  
156 (SIF) and vegetation photosynthesis, validating SIF as an effective proxy for ecosystem  
157 gross primary productivity (GPP) (Li et al. 2018; Magney et al. 2019; Shekhar et al., 2022).  
158 The GOSIF dataset was created by training a Cubist Regression Tree model to gap-fill  
159 SIF retrievals from OCO-2 satellite. This was done using MODIS Enhanced Vegetation  
160 Index (EVI) and meteorological reanalysis data from MERRA-2 (Modern-Era  
161 Retrospective analysis for Research and Applications), which includes photosynthetically  
162 active radiation (PAR), VPD, and air temperature (see Li and Xiao, 2019). We  
163 downloaded GOSIF data set (v2) from the Global Ecology Data Repository  
164 ([http://data.globalecology.unh.edu/data/GOSIF\\_v2/](http://data.globalecology.unh.edu/data/GOSIF_v2/), last accessed on 25 July 2024). The  
165 GOSIF was available from 2000-2022 at 8-day temporal scale with a spatial resolution of  
166  $0.05^{\circ} \times 0.05^{\circ}$  (Li and Xiao, 2019).

167 GOSIF signals provide information about physiological response of forest photosynthesis  
168 while NIR<sub>v</sub> (a recently developed vegetation index) signals provide information about the  
169 health status of the canopy. NIR<sub>v</sub> is preferred over NDVI and EVI as it can isolate the  
170 vegetation signal, mitigate mixed-pixel issue, and partly address the influences of  
171 background brightness and soil contamination (Zhang et al. 2022). The two vegetation  
172 proxies used in this study are anticipated to offer complementary insights into vegetation  
173 response to drought.

#### 174 *Land cover dataset*

175 In this study, we focused on five different types of forests (and woodlands) across Europe,  
176 namely, evergreen needleleaf forest (ENF), evergreen broadleaf forest (EBF), deciduous

177 broadleaf forest (DBF), mixed forest (MF), and woody savannas (WSA). The spatial  
178 distribution of the five different forest types across Europe is shown in Figure 1. We used  
179 the yearly MODIS land cover product (MCD12C1 version 6.1 at  $0.05^\circ \times 0.05^\circ$  resolution)  
180 for the years of 2001, 2006, 2011, 2016 and 2021, to extract total areas covered by each  
181 forest type. Area of each grid cell was calculated using trigonometric equations  
182 considering the latitudinal and longitudinal variations arising due to Earth's spherical  
183 shape (Ellipsoid). Only areas that were consistently identified as each forest type over the  
184 five-year period were included in the analysis. This means that only pixels common  
185 across these five years were selected, and with more than 50% of the  $0.05^\circ \times 0.05^\circ$  pixel  
186 area identified as forests. The forested areas selected for this study encompassed  
187 907,875 km<sup>2</sup>, which represents approximately 24% of Europe's total land area. Out of the  
188 total area about 23% (206'212 km<sup>2</sup>) was dominated by ENFs distributed largely across  
189 Northern Europe (NEU). Approximately 1% (7'000 km<sup>2</sup>) of the area was dominated by  
190 EBFs, located entirely in Mediterranean Europe (MED), and about 10% (92'209 km<sup>2</sup>) was  
191 dominated by DBF which was largely distributed across MED. Approximately 20%  
192 (174'934 km<sup>2</sup>) of the total forested area was dominated by MFs largely dominating Central  
193 Europe (CEU), and about 47% (427'529 km<sup>2</sup>) was dominated by WSA mostly found in  
194 NEU (Figure 1).

#### 195 *Drought detection and statistical data analysis*

196 The focus of our analysis was on the summer months during three extreme years of 2003,  
197 2018, and 2022. For this purpose, we subset VPD, soil moisture (SM), and both  
198 vegetation proxies (NIRv and GOSIF) for the months of June, July, August (JJA) which  
199 consisted of fourteen 8-day periods, for each forested pixel between 2000 and 2022. We  
200 restricted our analysis to the months of June-July-August so our study is 1) comparable  
201 with existing studies focused on the summer drought 2) to capture the peak of the warm  
202 and dry conditions across Europe, that would be most stressful for the vegetation  
203 functioning, from the perspective of heat and water supply.

204 To account for the impact of the observed greening trend across Europe on vegetation  
205 proxy anomalies during the extreme years (2003, 2018, 2022), we applied a detrending  
206 process to the summer mean NIRv and GOSIF data. This detrending was performed

207 pixel-wise from 2000 to 2022 using a simple linear regression model (Buras et al., 2020).  
208 We then calculated pixel-wise standardized summer anomalies, expressed as z-scores  
209 ( $Var_z$ ), for all variables—VPD, SM, and the detrended NIRv and GOSIF (hereafter  
210 referred to as NIRv and GOSIF)—for each year, including the extreme years, using  
211 Equation 3.

212

$$213 \quad Var_z (\textit{unitless}) = \frac{Var - Var_{mean}}{Var_{sd}} \quad (3)$$

214

215 where,  $Var_{mean}$  and  $Var_{sd}$  are mean and standard deviation of any variable over the 2000-  
216 2022 period.

217

218 In drought identification studies, classification of ‘normal’ (not to be confused with normal  
219 distribution), ‘drought’ (used synonymously with ‘dry’), or ‘wet’, is largely done using a  
220 standardized index, such as SPI (Standardized Precipitation Index), SPEI (Standardized  
221 Precipitation Evapotranspiration Index), and z-score among others (see Mishra and  
222 Singh, 2011). All studies that use a standardized index for classification, classify “normal”  
223 conditions when the index is between -1 and 1, and “below normal” conditions when the  
224 index is  $< -1$ , and “above normal” conditions when the index  $> 1$  (Jain et al., 2015, Wable  
225 et al., 2019, Dogan et al., 2012, Tsakiris and Vangelis, 2005). In this study, we classified  
226 drought conditions as occurring when soil moisture is below normal ( $SMz < -1$ ) and VPD  
227 is above normal ( $VPDz > 1$ ), indicating both soil AND atmospheric dryness. This  
228 threshold-based approach using standardized anomalies aligns with established methods  
229 for drought identification and is pertinent for studying drought impacts on forests. Both  
230 soil moisture and VPD directly affect vegetation functioning, making them effective  
231 proxies for identifying environmental constraints on plant physiological performance.  
232 Furthermore, such classification of ‘normal’ (and thus, ‘above normal’ and ‘below normal’  
233 used in this study) based on z-scores (also called standardized anomalies) can be done  
234 for any meteorological and/or response variables, such as NIRv and GOSIF done in this  
235 study, making the narration of results coherent across different variables.

236 We used the Pearson correlation coefficient ( $r$ ) and partial correlation coefficients (Pr) to  
237 understand the spatial (across space for each year) and temporal (during each year)



238 correlation of GOSIF and NIR<sub>v</sub> anomalies with SM and VPD anomalies (Dang et al.,  
239 2022). We calculated the partial correlation coefficient using equations 4-7:

240

$$241 \quad Pr(GOSIF, SM) = \frac{r(GOSIF, SM) - r(GOSIF, VPD) \times r(SM, VPD)}{\sqrt{1 - r(GOSIF, VPD)^2} - \sqrt{1 - r(SM, VPD)^2}} \quad (4)$$

242

$$243 \quad Pr(GOSIF, VPD) = \frac{r(GOSIF, VPD) - r(GOSIF, SM) \times r(SM, VPD)}{\sqrt{1 - r(GOSIF, SM)^2} - \sqrt{1 - r(SM, VPD)^2}} \quad (5)$$

244

$$245 \quad Pr(NIRv, SM) = \frac{r(NIRv, SM) - r(NIRv, VPD) \times r(SM, VPD)}{\sqrt{1 - r(NIRv, VPD)^2} - \sqrt{1 - r(SM, VPD)^2}} \quad (6)$$

246

$$247 \quad Pr(NIRv, VPD) = \frac{r(NIRv, VPD) - r(NIRv, SM) \times r(SM, VPD)}{\sqrt{1 - r(NIRv, SM)^2} - \sqrt{1 - r(SM, VPD)^2}} \quad (7)$$

## 248 **Results**

### 249 *Severity of the 2022 summer drought compared to 2018 and 2003*

250 Figure 2 shows the extent and magnitude of anomalies (z-score) of VPD and top layer (0-  
251 7 cm) soil moisture content during the summer months in 2003, 2018, and 2022 across  
252 Europe. In summer 2022, particularly southern regions of Europe experienced the most  
253 pronounced increase in atmospheric (z-score > 1) and soil dryness (z-score < -1) (Figure  
254 2) while in 2018 we observed the most widespread VPD and SM anomalies in northern  
255 Europe (Figure 2).

256 Figure 3 shows the intensity of atmospheric and soil drought via z-score values of VPD  
257 and SM anomalies over the summer months (JJA) in 2003, 2018, and 2022. The total  
258 affected area displayed in Figure 3 is the sum of all pixels within the given z-score bin  
259 during the summer period where z-scores are averaged for each bin for the summer  
260 period. Restricted to forested areas, atmospheric and soil drought was 55% and 58%  
261 more extensive in 2018 compared to 2022, and in both years more extensive than in 2003  
262 (Figure 3). In 2022, 28 Mha of forested areas in Europe experienced an extremely high  
263 VPD (z-score > 1), while in 2018, 63 Mha experienced such extreme conditions. In 2022,  
264 21 Mha of forested areas experienced an extremely low soil moisture content (z-score <

265 -1) while in 2018, 50 Mha of forests in Europe were affected by such extreme conditions.  
266 In 2003 an area of 25 Mha was affected by extremely dry air and a similar area was  
267 affected by extremely dry soil (Figure 3). A comparison of soil drought detected from SM  
268 at 0-100 cm showed a similar result in terms of drought severity and spatial coverage and  
269 thus we used SM at 0-7 cm soil layer for our analysis (see Supplementary Figure 1).

270

### 271 *Forest canopy response to the 2022 drought*

272 The intensity of GOSIF and NIRv anomalies over the summer months (JJA) in 2003,  
273 2018, and 2022 are displayed in Figure 4. The extent shown in Figure 4 is the sum of all  
274 pixels within the given z-score bin during the summer period (z-scores are averaged for  
275 each bin). Compared to 2018, the extremely dry conditions in 2022 led to 30% increase  
276 in forested areas that exhibited declined photosynthesis (17 Mha in 2022 compared to 12  
277 Mha in 2018) (Figure 4). The extent of the canopy browning observed in 2022 was similar  
278 to 2018, which in both years was 120% of the extent of observed canopy browning in  
279 2003 (11 Mha compared to 5 Mha observed in 2003) (Figure 4).

280 Figure 5a shows the GOSIF anomalies (z-score) across all forested areas in Europe. The  
281 intensity and extent of the GOSIF anomalies during the summer months (JJA) in each  
282 year are shown for different forest types in Figure 5b. Across specific forest types, DBFs  
283 showed the largest negative GOSIF anomaly in 2022 but the ENFs showed a positive  
284 GOSIF anomaly in 2022, both in terms of magnitude and in terms of the spatial extent of  
285 negative GOSIF anomalies (Figure 5).

286 Figure 6a shows the anomalies of NIRv (average z-score over the summer months)  
287 across all forested areas in Europe. The intensity and extent of the NIRv anomalies during  
288 the summer months (JJA) in each year are shown for different forest types in Figure 6b.  
289 In terms of canopy browning response (NIRv anomalies), the largest negative NIRv  
290 anomalies in 2022 were observed in southern Europe (Figure 6). Largest negative NIRv  
291 anomalies (indicated by the maximum anomaly) were observed in the DBFs in 2022,  
292 fitting the declined GOSIF signals. The ENFs showed positive NIRv anomalies in 2022,  
293 in terms of magnitude, spatial coverage, and % of total area affected (Figure 6).

294

### 295 *Relationship between GOSIF and NIRv*

296 In general, the values of NIRv and GOSIF were highly correlated (Supplementary Figure  
297 2). The anomalies of NIRv and GOSIF were most correlated across WSAs ( $r^2 = 0.73$  in  
298 2018) and least correlated across the ENFs (Supplementary Figure 2). Figure 7 shows  
299 the spatial regression between standardized GOSIF anomalies with (a) VPD and (b) SM  
300 and Figure 8 shows the spatial regression between standardized NIRv anomalies with (a)  
301 VPD and (b) SM over the drought areas in summers 2003, 2018 and 2022. With the  
302 increase in VPD (i.e., increased atmospheric dryness), GOSIF values declined across all  
303 forest types, across all years, except in 2022 in the WSA, and in 2018 and 2022 in EBFs  
304 (Figure 7). With decrease in soil moisture (i.e., increased soil dryness), GOSIF values  
305 also declined overall ( $r^2 = 0.34$ ), but not as strongly as with the increase in air dryness ( $r^2$   
306  $= 0.39$ ) (Figure 7). Across different forest types, GOSIF responded most strongly to VPD  
307 anomalies in the MFs (mean  $r^2 = 0.48$ ), and responded most directly to changes in the  
308 soil moisture in the WSA (Figure 7).

309 Between VPD and SM, in general GOSIF anomalies were more correlated with VPD than  
310 with SM anomalies, and the decline in VPD correlated well with the larger GOSIF decline  
311 that we observed in DBFs in 2022 and in ENFs in 2003 (Figure 7). Under typical  
312 conditions (regardless of drought), GOSIF's response to both air dryness and soil  
313 moisture anomalies was more pronounced than the response of NIRv ( $r^2 = 0.39$  with  
314 GOSIF, compared to  $r^2 = 0.29$  for NIRv) (Figure 7, 8).

315 Figure 9 shows the partial correlation coefficient between GOSIF with SM and VPD during  
316 summer months (JJA) for areas identified as affected (Figure 9a) and not affected (Figure  
317 9b) by drought. The SM and VPD values across all forest types correlated well, but across  
318 DBFs the dryness in the atmosphere and the dryness in the soil were most correlated  
319 (Figure 9). Regarding canopy response to VPD, European Needleleaf Forests (ENF)  
320 exhibited the strongest reaction to changes in atmospheric dryness (Figure 9)

## 321 **Discussion**

### 322 *Severity of the 2022 summer drought*

323 Although the years 2003, 2018, and 2022 are all categorized as "extreme," the specific  
324 characteristics of the extreme conditions varied significantly among these years. For

325 example, in 2003, widespread negative anomalies in soil moisture signaled a significant  
326 soil drought, whereas in 2022, widespread positive VPD anomalies indicated a notably  
327 drier atmosphere (Figure 3). It is important to note that ERA-5 Land datasets have been  
328 shown to underestimate the extent of European heatwaves in 2003, 2010, and 2018  
329 (Duveiller et al., 2023), partly due to the use of a static leaf area index in their modeling  
330 framework. Consequently, the SM droughts in the years 2003, 2018, and 2022 may be  
331 more severe than indicated by our study, suggesting that our results might be somewhat  
332 conservative. The extensive summer drought in 2022 primarily impacted southern  
333 Europe, in contrast to the 2003 summer drought, which affected central Europe, and the  
334 2018 drought, which extended to central and northern Europe (Figure 2) (Bastos et al.,  
335 2020). Consequently, the severe dry conditions in 2022 resulted in an average decline in  
336 GOSIF across forests that was 30% more widespread compared to 2018, and 60% more  
337 widespread compared to 2003 (Figure 4). These above-normal dry conditions during the  
338 summer reduced the photosynthetic capacity of plants and, consequently, the  
339 ecosystem's ability to absorb carbon from the atmosphere (Peters et al., 2018; van der  
340 Woude et al., 2023). Although the atmospheric and soil droughts in 2018 were more  
341 extensive and severe compared to 2022 (as indicated by the maximum observed z-  
342 scores), the adverse impact on forests, as reflected by the decline in GOSIF, was greater  
343 in 2022.

#### 344 *Canopy response to soil versus atmospheric dryness*

345 The GOSIF dataset used in this study has been shown to be a reliable proxy for  
346 vegetation gross productivity, as demonstrated by comparisons with ground-based flux  
347 measurements (Shekhar et al. 2022; Pickering et al. 2022). It is important to note that  
348 GOSIF estimates are derived from a machine learning model trained with OCO-2 SIF  
349 observations, MODIS EVI data, and meteorological reanalysis data. As a result, the  
350 meteorological data used in our analyses are not entirely independent of the SIF data.  
351 However, this overlap is unlikely to impact our findings. A recent study that compared  
352 GOSIF with original OCO-2 data to assess the impacts of the 2018 U.S. drought found  
353 similar responses to drought between the two datasets (Li et al., 2020).

354 NIRv and SIF signals are well-correlated and effectively capture seasonal patterns in GPP  
355 (Getachew Mengistu et al. 2021). Although the strength of their relationship can vary with  
356 time, location, and forest type (see Supplementary Figure 2), reductions in SIF signals  
357 are directly associated with decreased photosynthesis. While both SIF and NIRv are  
358 reliable indicators of canopy responses to extreme climate events, SIF is more responsive  
359 to short-term climatic changes (Figure 7).

360 Our analysis showed that across different regions, GOSIF anomalies corresponded more  
361 strongly to increased atmospheric dryness than to increased soil dryness (Figure 7). This  
362 supports the understanding that vapor pressure deficit plays a larger role in controlling  
363 SIF signals for trees over shorter time scales than soil moisture (Pickering et al. 2022).  
364 Over shorter time frames, trees can often mitigate soil moisture deficits through  
365 mechanisms within the rooting zone and by accessing deeper water sources, whereas  
366 there is no such buffer for the impact of atmospheric dryness on tree canopies.

367 Ground-based observations in forest ecosystems, including both ecosystem and tree-  
368 level measurements, have shown that atmospheric dryness can constraint canopy gas  
369 exchange, even when soil moisture is not limiting (Gharun et al. 2014, Fu et al. 2022,  
370 Shekhar et al. 2024a). These findings highlight the importance of considering atmospheric  
371 dryness as a limiting factor for tree photosynthesis during extremely dry conditions and  
372 demonstrate the rapid response of various canopy types to increased levels of  
373 environmental dryness.

#### 374 *Canopy response to drought across different forest types*

375 The spread of drought, measured as the total area across z-scores, exhibited distinct  
376 patterns in different years, leading to varied responses of different forest types to the  
377 climatic anomalies. Impact of drought on forests can significantly differ depending on the  
378 forest type, tree species, species composition, and past exposure to extreme conditions  
379 (Arthur and Dech 2016; Chen et al. 2022). Our analysis showed that conditions in summer  
380 2022 reduced vegetation functioning across DBFs the most, as it was indicated by  
381 declined GOSIF signals (Figure 5). While deciduous broad-leaved forests were most  
382 negatively affected by the extreme conditions in 2022, Evergreen Needle-Leaf Forests  
383 (ENF) distributed in northern regions of Europe were not exposed to extremely dry  
384 conditions in 2022 and even showed enhanced canopy greening and GOSIF signals,

385 through benefiting from the episodic warming (Forzieri et al. 2022). Under similar drought  
386 conditions, the mechanisms to cope with the level of drought stress vary largely among  
387 forest types, and depend on a combination of characteristics that control water loss  
388 through the coordination of stomatal regulation, hydraulic architecture, and root  
389 characteristics (e.g., rooting depth, root distribution, root morphology) (Gharun et al. 2020;  
390 Peters et al. 2023). Stomata of trees exhibit a high sensitivity to VPD fluctuations, causing  
391 a reduction in stomatal conductance as VPD increases, which, in turn, limits the exchange  
392 of CO<sub>2</sub> with the atmosphere during photosynthesis (Bonal and Guehl in 2011; Li et al.  
393 2023). Different tree species show varying degrees of sensitivity in their stomatal  
394 responses to atmospheric dryness (Oren et al., 1999). For example, ring-porous species  
395 tend to maintain robust gas exchange under dry conditions, while diffuse-porous species,  
396 like those in ENFs, exhibit stronger stomatal regulation, reducing stomatal conductance  
397 as water availability decreases (Klein, 2014). This variability places plants on a spectrum  
398 of drought tolerance, reflecting their specific water relations strategies and leading to  
399 different responses among forests in similar climatic regions.

#### 400 *Vulnerability of forests to more frequent drought*

401 The increased canopy damage observed in 2022, despite less severe conditions  
402 compared to the previous extreme year, suggests a lasting impact on forest canopies that  
403 could lead to a decline in forest resilience in the face of more frequent drought events  
404 (Forzieri et al., 2022). A potential decline in the resilience of forests has significant  
405 implications for vital ecosystem services, including the forest's capacity to mitigate climate  
406 change. Consequently, there is an urgent need to consider these trends when formulating  
407 robust forest-based mitigation strategies. This need is especially critical given future  
408 projections indicating that the frequency and intensity of extreme dryness across Europe  
409 will more than triple by the end of the 21st century (Shekhar et al., 2024b). In this context,  
410 it is increasingly important to investigate the vulnerability of forests to external  
411 perturbations and to develop mitigation strategies tailored to site-specific  
412 ecophysiological and environmental factors that influence forest resilience to drought.  
413 Effective management strategies should be based on an understanding of these factors

414 to mitigate the legacy effects of drought (McDowell et al., 2020; Wang et al., 2023;  
415 Shekhar et al., 2024a).

416

#### 417 **Conclusion**

418 The severity of the 2022 summer drought, marked by increased atmospheric dryness,  
419 significantly compromised the photosynthetic capacity of trees, leading to widespread  
420 declines in vegetation functioning, especially in deciduous broad-leaved forests. Our  
421 findings underscore the importance of considering atmospheric dryness as a critical factor  
422 influencing canopy responses during extreme climatic events, alongside soil moisture  
423 deficits. Despite less severe overall conditions compared to previous extreme years, the  
424 greater canopy damage observed in 2022 suggests a growing vulnerability of forests to  
425 drought. This raises concerns about the future climate mitigation capacity of forest  
426 ecosystems, particularly as projections indicate a continued increase in the frequency and  
427 intensity of extreme dryness across Europe.

428

#### 429 **Competing interests**

430 The authors have no competing interests to declare.

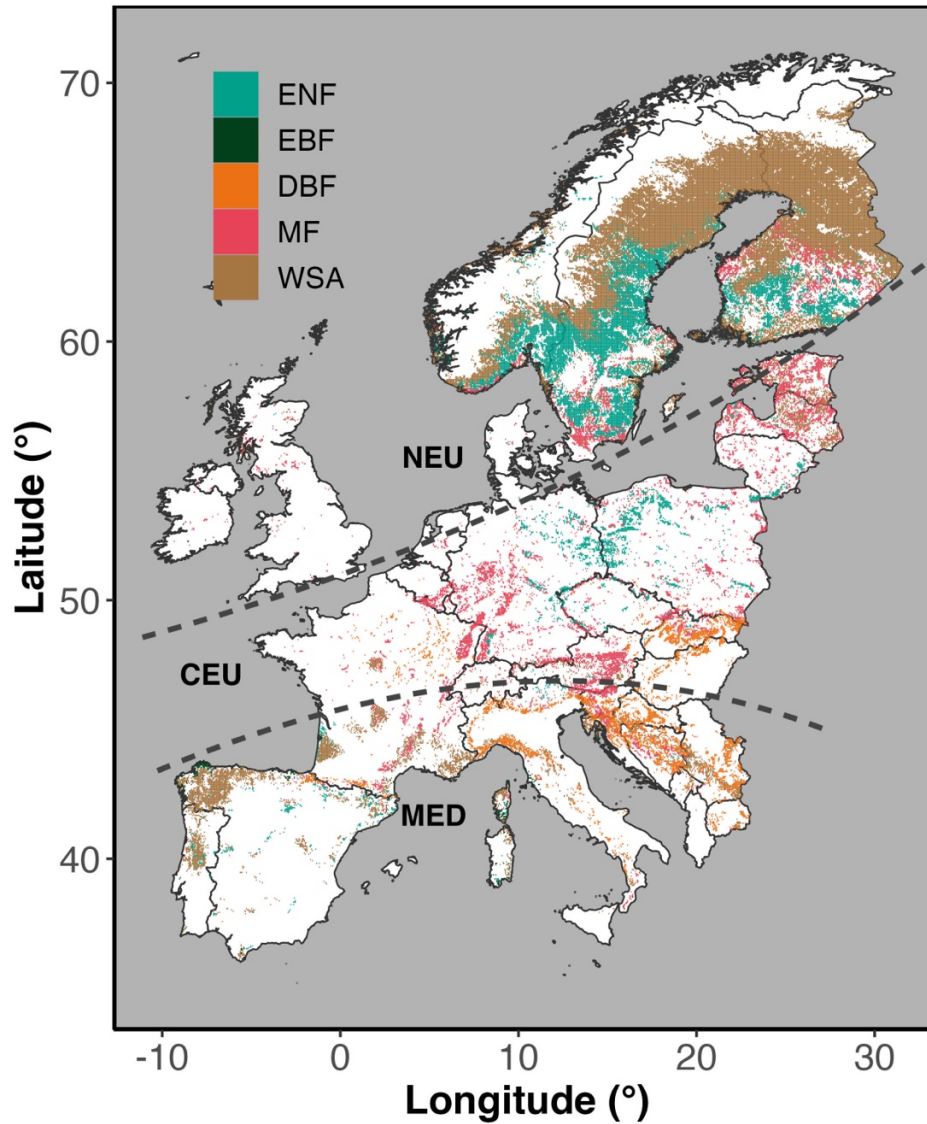
431

#### 432 **Financial support**

433 AS acknowledges funding from the SNF funded project EcoDrive (IZCOZ0\_198094). JX  
434 was supported by the National Science Foundation (NSF) (Macrosystem Biology &  
435 NEON-Enabled Science program: DEB-2017870).

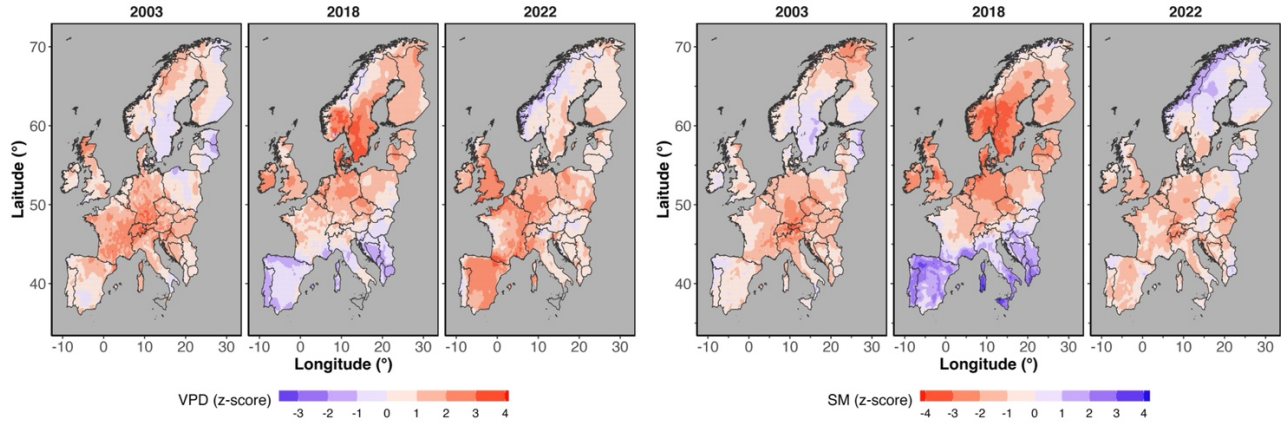
436 **Data availability** The R scripts used for the data analyses and plots are available upon  
437 request from the corresponding author.

438 **Author contributions** MG, AS, NB conceptualized the study. AS, JX, XL: data  
439 processing. MG and AS: data analyses. MG, AS, JX, XL: paper writing, revision and  
440 editing of the paper.



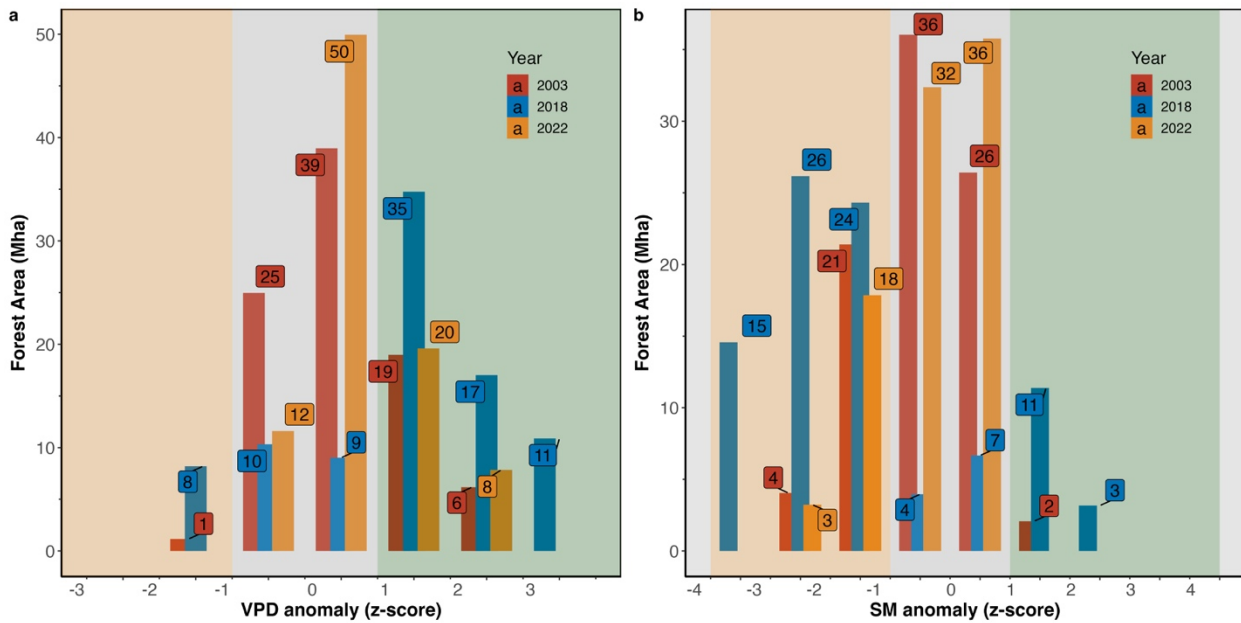
441  
 442 **Figure 1** Spatial coverage of forests (ENF - evergreen needleleaf forest; EBF - evergreen  
 443 broadleaf forest; DBF - deciduous broadleaf forest; MF - mixed forest), and woodlands  
 444 (WSA - woody savannas) across Europe. Areas are differentiated into Northern Europe  
 445 (NEU), Central Europe (CEU), and Mediterranean Europe (MED) following Markonis et  
 446 al. (2021). The map is based on MODIS land cover product MCD12C1 (version 6.1).



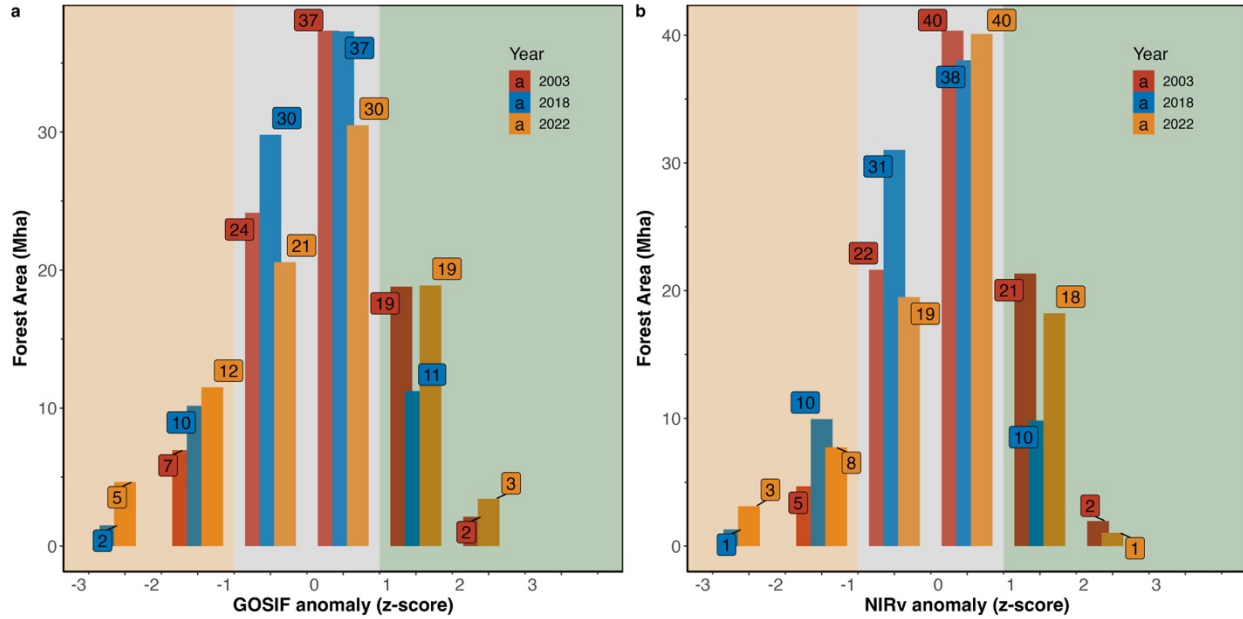


447  
 448 **Figure 2** Standardized summer (JJA) anomalies (z-score) of mean vapor pressure deficit  
 449 (VPD), and top layer (0-7 cm depth) soil moisture (SM) in 2003, 2018 and 2022, across  
 450 the region of Europe.

451  
 452  
 453

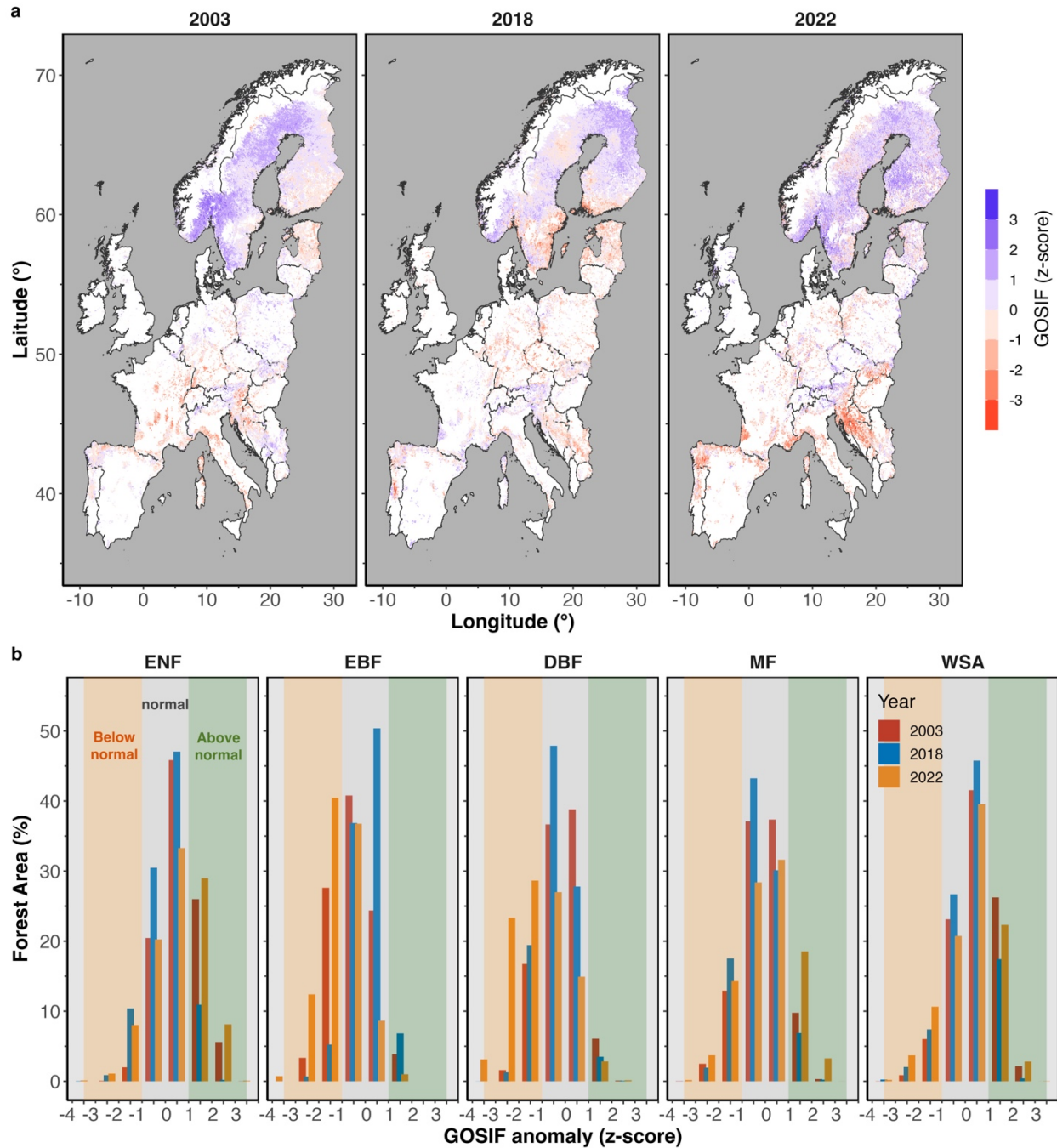


454  
 455  
 456 **Figure 3** Intensity (z-score) and extent (area affected, Mha) of (a) VPD, and (b) SM  
 457 anomalies across forested areas during the summer months (JJA). Z-score, values from  
 458 -1 and 1 are considered normal (within 1 standard deviation of the mean). Orange-shaded  
 459 area marks below normal and green-shaded area marks above normal conditions.

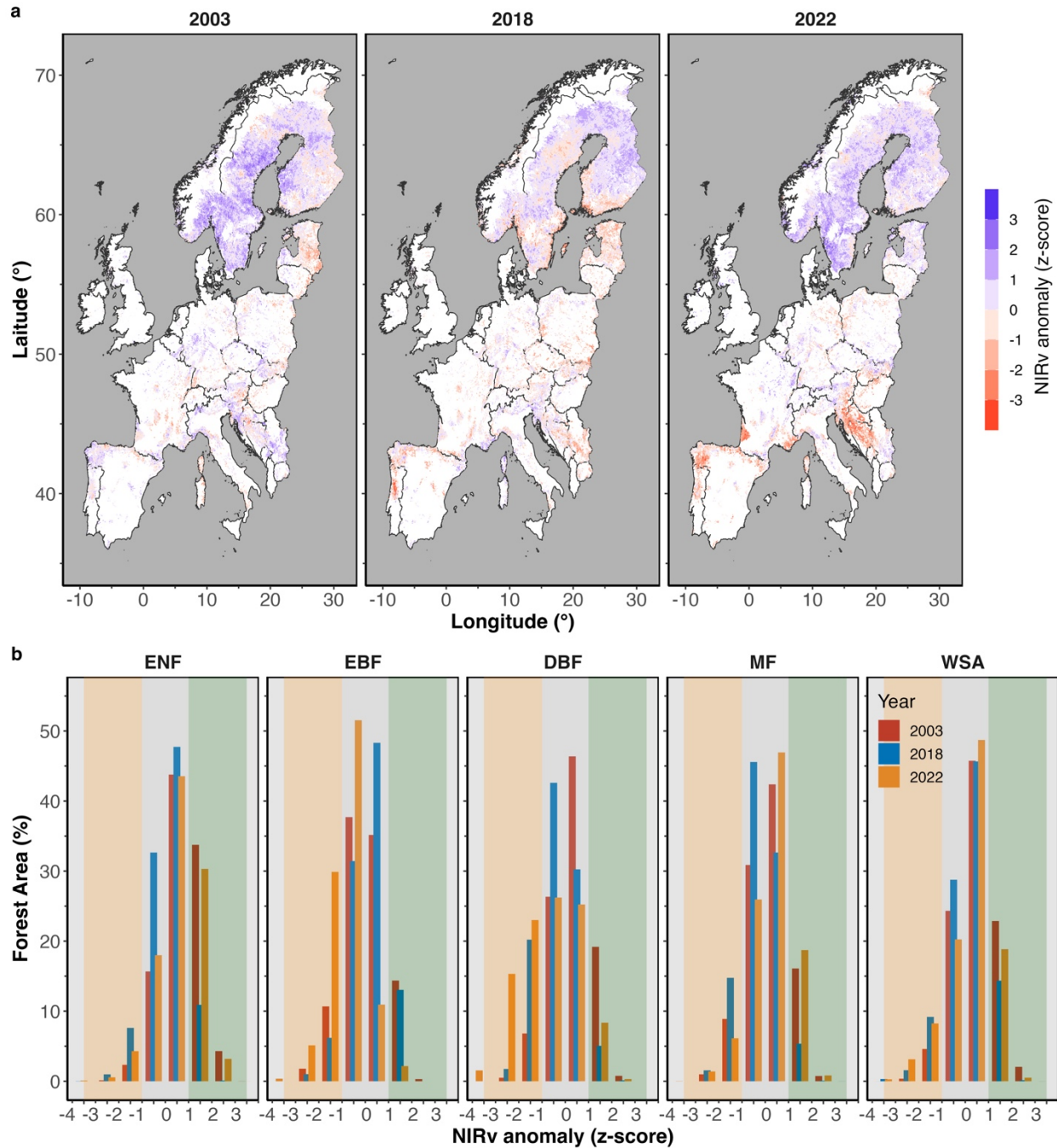


460  
461  
462  
463  
464  
465  
466

**Figure 4** Intensity (z-score) and extent (area affected, Mha) for (a) GOSIF, and (b) NIRv anomalies across forested areas during the summer months (JJA). Z-score, values from -1 and 1 are considered normal (within 1 standard deviation of the mean). Orange-shaded area marks below normal and green-shaded area marks above normal conditions.



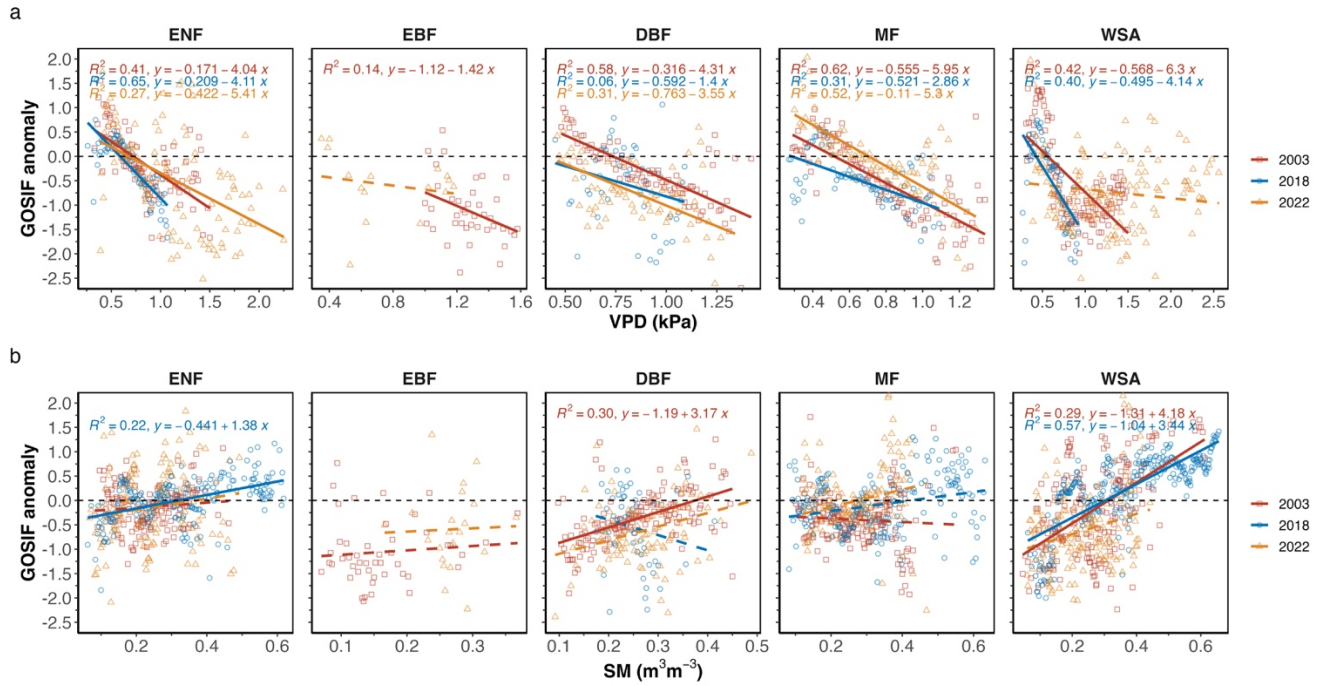
467  
 468 **Figure 5** (a) GOSIF anomaly (in terms of z-score) across Europe, and (b) area coverage  
 469 (in terms of percentage of total area for each forest type) during the summer months (JJA)  
 470 in 2003, 2018 and 2022. Orange-shaded area marks below normal and green-shaded  
 471 area marks above normal conditions. White areas on the map mark non-forested regions.  
 472  
 473



474

475

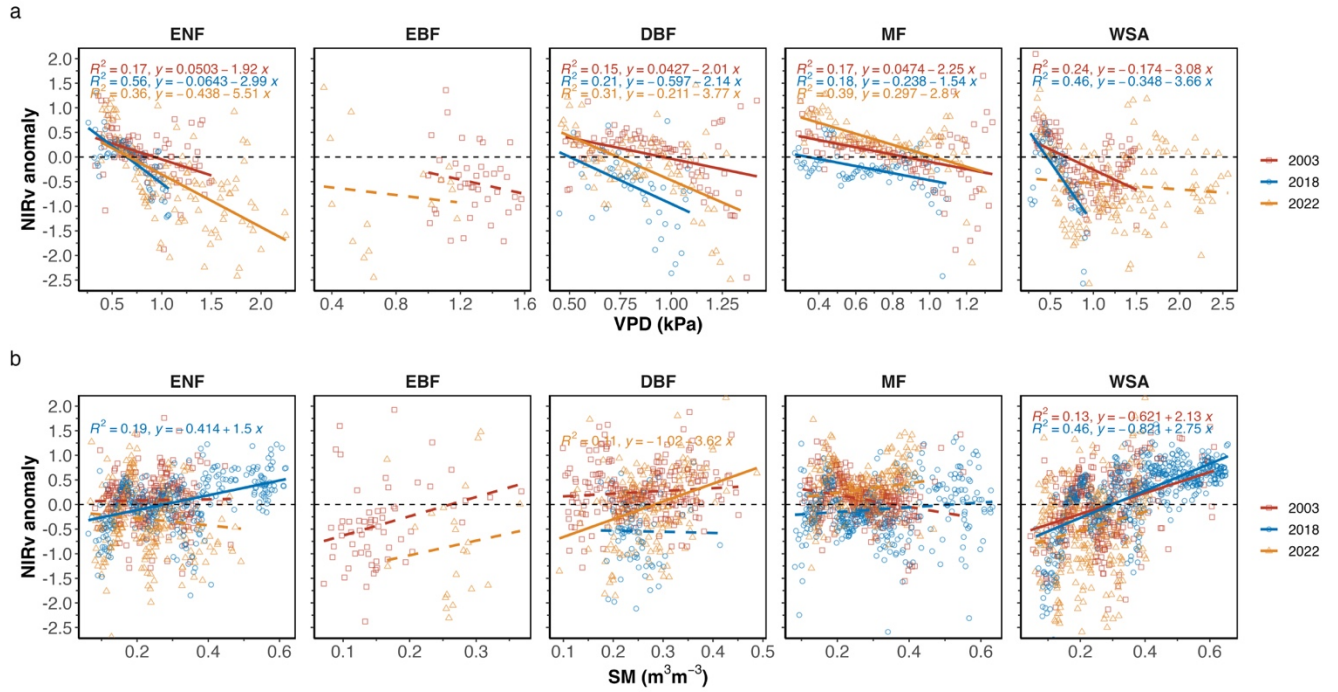
476 **Figure 6** (a) NIRv anomaly (in terms of z-score) across Europe, and (b) area coverage  
 477 (in terms of percentage of total area for each forest type) during the summer months (JJA)  
 478 in 2003, 2018 and 2022. In panel (b) Orange-shaded area marks below normal and green-  
 479 shaded area marks above normal conditions. White areas on the map mark non-forested  
 480 regions.



481  
 482  
 483  
 484  
 485  
 486  
 487

**Figure 7** Spatial regression between standardized GOSIF anomalies with (a) VPD and (b) SM over the drought areas during the summer months (JJA) 2003, 2018 and 2022. Dashed lines mark a non-significant relationship ( $p > 0.05$ ).





488

489

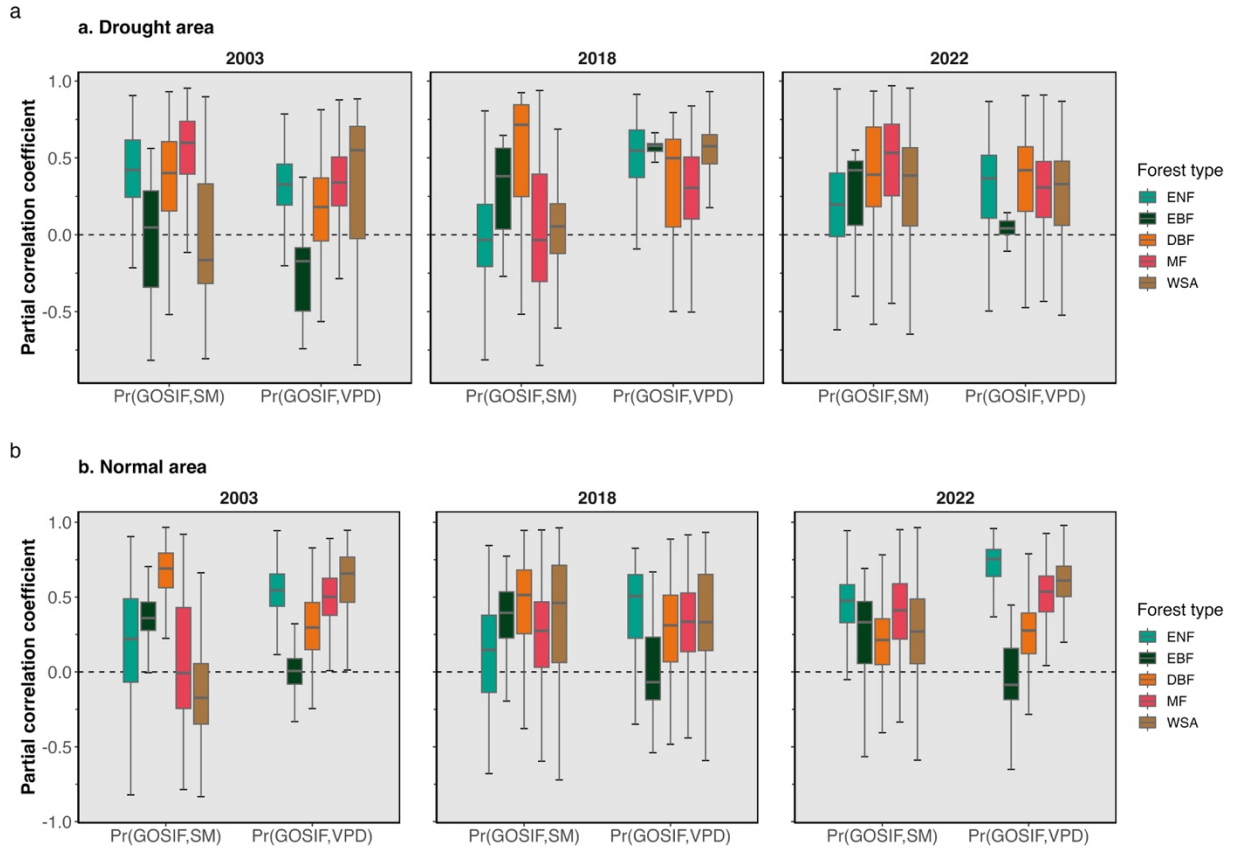
490 **Figure 8.** Spatial (over all pixels) regression between standardized NIRv anomalies with  
 491 (a) VPD and (b) SM over the drought areas and normal areas in 2003, 2018, and 2022  
 492 during the summer months (JJA).

493

494

495

496



497

498 **Figure 9.** Temporal partial correlation coefficient of GOSIF with the absolute values of  
 499 SM and VPD during the summer months (JJA) in 2003, 2018 and 2022, for detected (a)  
 500 drought areas and (b) normal areas. A comparable figure for NIRv can be found in  
 501 Supplementary Figure 3.

502

503

504 **References**

- 505 Albergel, C., De Rosnay, P., Balsamo, G., Isaksen, L., Munoz-Sabater, J., 2012. Soil  
506 moisture analyses at ECMWF: evaluation using global ground-based in situ  
507 observations. *J. Hydrometeorol.* 13, 1442–1460. <https://doi.org/10.1175/JHM-D11-0107.1>.
- 508 Anjileli, H., Huning, L.S., Moftakhari, H. et al. (2021) Extreme heat events heighten soil  
509 respiration. *Sci Rep* 11, 6632. <https://doi.org/10.1038/s41598-021-85764-8>
- 510 Arthur CM, Dech JP (2016) Species composition determines resistance to drought in dry forests  
511 of the Great Lakes - St. Lawrence forest region of central Ontario. *Journal of Vegetation Science*  
512 27, 914-925.
- 513 Badgley G et al. (2017) Canopy near-infrared reflectance and terrestrial photosynthesis. *Sci.*  
514 *Adv.* 3, e1602244. DOI:10.1126/sciadv.1602244
- 515 Bastos A et al. (2020) Impacts of extreme summers on European ecosystems: a comparative  
516 analysis of 2003, 2010 and 2018. *Phil. Trans. R. Soc. B* 375: 20190507.  
517 <http://dx.doi.org/10.1098/rstb.2019.0507>
- 518 Bauke, S. L., Amelung, W., Bol, R., Brandt, L., Brüggemann, N., Kandeler, E., Meyer, N., Or,  
519 D., Schnepf, A., Schloter, M., Schulz, S., Siebers, N., von Sperber, C., & Vereecken, H. (2022).  
520 Soil water status shapes nutrient cycling in agroecosystems from micrometer to landscape  
521 scales. *Journal of Plant Nutrition and Soil Science*, 185, 773–792.  
522 <https://doi.org/10.1002/jpln.202200357>
- 523 Bonal, D. & Guehl, J.-M. (2011) Contrasting patterns of leaf water potential and gas exchange  
524 responses to drought in seedlings of tropical rainforest species. *Functional Ecology*, 15, 490–  
525 496.
- 526 Buras, A., Rammig, A., and Zang, C. S. (2020) Quantifying impacts of the 2018 drought on  
527 European ecosystems in comparison to 2003, *Biogeosciences*, 17, 1655–1672,  
528 <https://doi.org/10.5194/bg-17-1655-2020>.
- 529 Chen, Y., Vogel, A., Wagg, C. et al. (2022) Drought-exposure history increases complementarity  
530 between plant species in response to a subsequent drought. *Nat Commun* 13, 3217.  
531 <https://doi.org/10.1038/s41467-022-30954-9>
- 532 Choat, B., Brodribb, T.J., Brodersen, C.R. et al. (2018) Triggers of tree mortality under drought.  
533 *Nature* 558, 531–539. <https://doi.org/10.1038/s41586-018-0240-x>
- 534 Cornes, R. C., van der Schrier, G., van den Besselaar, E. J. M., & Jones, P. D. (2018). An  
535 Ensemble Version of the E-OBS Temperature and Precipitation Data Sets. *Journal of*  
536 *Geophysical Research: Atmospheres*, 123(17), 9391–9409.  
537 <https://doi.org/10.1029/2017JD028200>



538 Dang, C., Shao, Z., Huang, X., Qian, J., Cheng, G., Ding, Q., & Fan, Y. (2022). Assessment of  
539 the importance of increasing temperature and decreasing soil moisture on global ecosystem  
540 productivity using solar-induced chlorophyll fluorescence. *Global Change Biology*, 28(6), 2066–  
541 2080. <https://doi.org/10.1111/gcb.16043>  
542

543 Dee, D. P., Uppala, S. M., Simmons, A. J., Berrisford, P., Poli, P., Kobayashi, S., Andrae, U.,  
544 Balmaseda, M. A., Balsamo, G., Bauer, P., Bechtold, P., Beljaars, A. C. M., van de Berg, L.,  
545 Bidlot, J., Bormann, N., Delsol, C., Dragani, R., Fuentes, M., Geer, A. J., Haimberger, L., Healy,  
546 S. B., Hersbach, H., Hólm, E. V., Isaksen, I., Kållberg, P., Köhler, M., Matricardi, M., McNally,  
547 A. P., Monge-Sanz, B. M., Morcrette, J. J., Park, B. K., Peubey, C., de Rosnay, P., Tavolato,  
548 C., Thépaut, J. N., and Vitart, F. (2011) The ERA-Interim reanalysis: configuration and  
549 performance of the data assimilation system, *Quarterly Journal of the Royal Meteorological*  
550 *Society*, 137, 121 553-597, [10.1002/qj.828](https://doi.org/10.1002/qj.828).

551 S. Dogan, A. Berktaç, V.P. Singh (2012) Comparison of multi-monthly rainfall-based drought  
552 severity indices, with application to semi-arid Konya closed basin, Turkey  
553 *J. Hydrol.*, 470–471, pp. 255-268  
554

555 Drake JE, Tjoelker MG, Vårhammar A, Medlyn BE, Reich PB, Leigh A, Pfautsch S, Blackman  
556 CJ, López R, Aspinwall MJ, Crous KY, Duursma RA, Kumarathunge D, De Kauwe MG,  
557 Jiang M, Nicotra AB, Tissue DT, Choat B, Atkin OK, Barton CVM (2018) Trees tolerate an  
558 extreme heatwave via sustained transpirational cooling and increased leaf thermal tolerance.  
559 *Glob Change Biol.* 24: 2390–2402. <https://doi.org/10.1111/gcb.14037>  
560

561 Duveiller, G., Pickering, M., Muñoz-Sabater, J., Caporaso, L., Boussetta, S., Balsamo, G., and  
562 Cescatti, A. (2023) Getting the leaves right matters for estimating temperature extremes,  
563 *Geosci. Model Dev.*, 16, 7357–7373, <https://doi.org/10.5194/gmd-16-7357-2023>.  
564

565 Forzieri, G., Dakos, V., McDowell, N.G. et al. (2022) Emerging signals of declining forest  
566 resilience under climate change. *Nature* 608, 534–539. [https://doi.org/10.1038/s41586-022-](https://doi.org/10.1038/s41586-022-04959-9)  
567 [04959-9](https://doi.org/10.1038/s41586-022-04959-9)  
568 Fu, Z., Ciais, P., Prentice, I.C. et al. Atmospheric dryness reduces photosynthesis along a large  
569 range of soil water deficits. *Nat Commun* 13, 989 (2022). [https://doi.org/10.1038/s41467-022-](https://doi.org/10.1038/s41467-022-28652-7)  
570 [28652-7](https://doi.org/10.1038/s41467-022-28652-7)  
571

572 Gessler, A., Bottero, A., Marshall, J. and Arend, M. (2020), The way back: recovery of trees  
573 from drought and its implication for acclimation. *New Phytol*, 228: 1704-1709.  
574 <https://doi.org/10.1111/nph.16703>  
575 Getachew Mengistu, A., Mengistu Tsidu, G., Koren, G., Kooreman, M. L., Folkert Boersma, K.,  
576 Tagesson, T., Ardö, J., Nouvellon, Y., & Peters, W. (2021). Sun-induced fluorescence and near-  
577 infrared reflectance of vegetation track the seasonal dynamics of gross primary production over  
578 Africa. *Biogeosciences*, 18(9), 2843-2857. <https://doi.org/10.5194/bg-18-2843-2021>

- 579 Gharun M., Vervoort R.W., Turnbull T.L., Adams M.A. (2014) A test of how coupling of  
580 vegetation to the atmosphere and climate spatial variation affects water yield modelling in  
581 mountainous catchments 514, pp. 202-213. <https://doi.org/10.1016/j.jhydrol.2014.04.037>
- 582 Gharun M., Hörtnagl L., Paul-Limoges E., Ghiasi S., Feigenwinter I., Burri S., Marquardt K.,  
583 Etzold S., Zweifel R., Eugster W., Buchmann N (2020) Physiological response of Swiss  
584 ecosystems to 2018 drought across plant types and elevation *Phil. Trans. R. Soc.*  
585 *B3752019052120190521*. <http://doi.org/10.1098/rstb.2019.0521>
- 586 Gourlez de la Motte L, Beauclaire Q, Heinesch B, Cuntz M, Foltýnová L, Šigut L, Kowalska N,  
587 Manca G, Ballarin IG, Vincke C, Roland M, Ibrom A, Lousteau D, Siebicke L, Neiryink J,  
588 Longdoz B. (2020) Non-stomatal processes reduce gross primary productivity in temperate  
589 forest ecosystems during severe edaphic drought. *Philos Trans R Soc Lond B Biol Sci.*  
590 *375(1810):20190527*. doi: 10.1098/rstb.2019.0527.
- 591 Haesen, S., Lembrechts, J. J., De Frenne, P., Lenoir, J., Aalto, J., Ashcroft, M. B., Kopecký, M.,  
592 Luoto, M., Maclean, I., Nijs, I., Niittynen, P., van den Hoogen, J., Arriga, N., Brúna, J.,  
593 Buchmann, N., Čiliak, M., Collalti, A., De Lombaerde, E., Descombes, P. ... Van Meerbeek, K.  
594 (2023). ForestClim—Bioclimatic variables for microclimate temperatures of European forests.  
595 *Global Change Biology*, 29, 2886–2892. <https://doi.org/10.1111/gcb.16678>
- 596 Humphrey V, Zscheischler J, Ciais P, Gudmundsson L, Sitch S, Seneviratne SI. (2018)  
597 Sensitivity of atmospheric CO<sub>2</sub> growth rate to observed changes in terrestrial water storage.  
598 *Nature*, 560 (7720): 628 DOI: 10.1038/s41586-018-0424-4.
- 599 Jain VK, Pandey RP, Jain MK, Byun HR (2015) Comparison of drought indices for appraisal of  
600 drought characteristics in the Ken River Basin, *Weather and Climate Extremes* 8, 1-11,  
601 <https://doi.org/10.1016/j.wace.2015.05.002>.
- 602 Klein Tank, A. M. G., Wijngaard, J. B., Können, G. P., Böhm, R., Demarée, G., Gocheva, A.,  
603 Mileta, M., Pashiardis, S., Hejkrlik, L., Kern-Hansen, C., Heino, R., Bessemoulin, P., Müller-  
604 Westermeier, G., Tzanakou, M., Szalai, S., Pálsdóttir, T., Fitzgerald, D., Rubin, S., Capaldo, M.,  
605 ... Petrovic, P. (2002). Daily dataset of 20th-century surface air temperature and precipitation  
606 series for the European Climate Assessment. *International Journal of Climatology*, 22(12),  
607 1441–1453. <https://doi.org/10.1002/joc.773>
- 608 Klein, T. (2014), The variability of stomatal sensitivity to leaf water potential across tree species  
609 indicates a continuum between isohydric and anisohydric behaviours. *Funct Ecol*, 28: 1313-  
610 1320. <https://doi.org/10.1111/1365-2435.12289>
- 611 Lal, P., Shekhar, A., Gharun, M., Das, N.N., 2023. Spatiotemporal evolution of global  
612 long-term patterns of soil moisture. *Sci. Total Environ.* 867, 161470 <https://doi.org/10.1016/j.scitotenv.2023.161470>.
- 613  
614
- 615 Lal, P., Singh, G., Das, N.N., Colliander, A., Entekhabi, D., 2022. Assessment of ERA5-  
616 land volumetric soil water layer product using in situ and SMAP soil moisture

617 observations. *Geosci. Rem. Sens. Lett. IEEE* 19, 1–5. [https://doi.org/10.1109/](https://doi.org/10.1109/LGRS.2022.3223985)  
618 [LGRS.2022.3223985](https://doi.org/10.1109/LGRS.2022.3223985).

619 Li X et al. (2018) Solar-induced chlorophyll fluorescence is strongly correlated with terrestrial  
620 photosynthesis for a wide variety of biomes: first global analysis based on OCO-2 and flux tower  
621 observations *Glob. Change Biol.* 24 3990–4008.

622

623 Li, X., Xiao, J. (2019) A global, 0.05-degree product of solar-induced chlorophyll fluorescence  
624 derived from OCO-2, MODIS, and reanalysis data. *Remote Sensing*, 11, 517;  
625 [doi:10.3390/rs11050517](https://doi.org/10.3390/rs11050517).

626 Li X, Xiao J, Kimball JS, Reichle RH, Frankenberg C (2020) Synergistic use of SMAP and OCO-  
627 2 data in assessing the responses of ecosystem productivity to the 2018 U.S. drought  
628 *Remote Sens. Environ.* 251, 112062

629

630 Li, F., Xiao, J., Chen, J., Ballantyne, A., Jin, K., Li, B., Abraha, M., John, R. (2023) Global water  
631 use efficiency saturation due to increased vapor pressure deficit. *Science*, 381, 672-677. DOI:  
632 [10.1126/science.adf5041](https://doi.org/10.1126/science.adf5041).

633

634 Magney T S et al. (2019) Mechanistic evidence for tracking the seasonality of photosynthesis  
635 with solar-induced fluorescence *Proc. Natl Acad. Sci. USA* 116 11640–5.

636

637 Marchin, R. M., Backes, D., Ossola, A., Leishman, M. R., Tjoelker, M. G., & Ellsworth, D. S.  
638 (2022). Extreme heat increases stomatal conductance and drought-induced mortality risk in  
639 vulnerable plant species. *Global Change Biology*, 28, 1133–1146.  
640 <https://doi.org/10.1111/gcb.15976>

641

642 Markonis, Y., Kumar, R., Hanel, M., Rakovec, O., Máca, P., AghaKouchak, A., (2021). The rise  
643 of compound warm-season droughts in Europe. *Science Advances* 7.  
644 <https://doi.org/10.1126/sciadv.abb9668>

645

646 McDowell, N. G. et al. (2020) Pervasive shifts in forest dynamics in a changing world. *Science*  
647 368, eaaz9463.

648

649 Mishra AK, Singh VP (2011) Drought modeling – A review, *Journal of Hydrology* 403(1–2),  
650 157-175, <https://doi.org/10.1016/j.jhydrol.2011.03.049>.

651

652 Müller, L. M., and M. Bahn (2022) Drought legacies and ecosystem responses to subsequent  
653 drought. *Global Change Biology* 28:5086–103. [doi:10.1111/gcb.16270](https://doi.org/10.1111/gcb.16270).

654

655 Muñoz-Sabater, J., Dutra, E., Agustí-Panareda, A., Albergel, C., Arduini, G., Balsamo, G.,  
656 Boussetta, S., Choulga, M., Harrigan, S., Hersbach, H., Martens, B., Miralles, D. G., Piles, M.,  
657 Rodríguez-Fernández, N. J., Zsoter, E., Buontempo, C., & Thépaut, J. N. (2021). ERA5-Land:  
658 A state-of-the-art global reanalysis dataset for land applications. *Earth System Science Data*,  
659 13(9), 4349–4383. <https://doi.org/10.5194/essd-13-4349-2021>

- 660 Peters, W., van der Velde, I.R., van Schaik, E. et al. Increased water-use efficiency and reduced  
661 CO<sub>2</sub> uptake by plants during droughts at a continental scale. *Nature Geosci* 11, 744–748  
662 (2018). <https://doi.org/10.1038/s41561-018-0212-7>
- 663 Peters, R.L., Steppe, K., Pappas, C., Zweifel, R., Babst, F., Dietrich, L., von Arx, G.,  
664 Poyatos, R., Fonti, M., Fonti, P., Grossiord, C., Gharun, M., Buchmann, N., Steger, D.N.  
665 and Kahmen, A. (2023), Daytime stomatal regulation in mature temperate trees  
666 prioritizes stem rehydration at night. *New Phytol*, 239: 533-546.  
667 <https://doi.org/10.1111/nph.18964>
- 668 Pickering, M., Cescatti, A., and Duveiller, G. (2022) Sun-induced fluorescence as a  
669 proxy for primary productivity across vegetation types and climates, *Biogeosciences*,  
670 19, 4833–4864, <https://doi.org/10.5194/bg-19-4833-2022>.
- 671 Oren, R., Sperry, J.S., Katul, G.G., Pataki, D.E., Ewers, B.E., Phillips, N. and Schäfer,  
672 K.V.R. (1999), Survey and synthesis of intra- and interspecific variation in stomatal  
673 sensitivity to vapour pressure deficit. *Plant, Cell & Environment*, 22: 1515-1526.  
674 <https://doi.org/10.1046/j.1365-3040.1999.00513.x>
- 675 Röthlisberger, M., Papritz, L. (2023). Quantifying the physical processes leading to  
676 atmospheric hot extremes at a global scale. *Nature Geosci.* 16(3), 210-216.  
677 doi:10.1038/s41561-023-01126-1.
- 678 Seidl, R., Thom, D., Kautz, M. et al. Forest disturbances under climate change. *Nature*  
679 *Clim Change* 7, 395–402 (2017). <https://doi.org/10.1038/nclimate3303>
- 680 Seneviratne, S. I., Zhang, X., Adnan, M., Badi, W., Dereczynski, C., Di Luca, A., Ghosh,  
681 S., Iskandar, I., Kossin, J., Lewis, S., Otto, F., Pinto, I., Satoh, M., Vicente-Serrano, S.  
682 M., Wehner, M., and Zhou, B. (2021) Weather and Climate Extreme Events in a  
683 Changing Climate, in: *Climate Change 2021: The Physical Science Basis. Contribution*  
684 *of Working Group I to the Sixth Assessment Report of the Intergovernmental Panel on*  
685 *Climate Change*, edited by: Masson-Delmotte, V., Zhai, P., Pirani, A., Connors, S. L.,  
686 Péan, C., Berger, S., Caud, N., Chen, Y., Goldfarb, L., Gomis, M. I., Huang, M., Leitzell,  
687 K., Lonnoy, E., Matthews, J. B. R., Maycock, T. K., Waterfield, T., Yelekçi, O., Yu, R.,  
688 and Zhou, B., Cambridge University Press, Cambridge, United Kingdom and New York,  
689 NY, USA, 1513–1766, <https://doi.org/10.1017/9781009157896.013>.
- 690 Shekhar, A., Hörtnagl, L., Buchmann, N., & Gharun, M. (2023). Long-term changes in  
691 forest response to extreme atmospheric dryness. *Global Change Biology*, 29, 5379–  
692 5396. <https://doi.org/10.1111/gcb.16846>

693 Shekhar A, Hörtnagl L, Paul-Limoges E, Etzold S, Zweifel R, Buchmann N, Gharun M  
694 (2024a) Contrasting impact of extreme soil and atmospheric dryness on the functioning  
695 of trees and forests. *Science of the Total Environment* 916, 169931.  
696 <https://doi.org/10.1016/j.scitotenv.2024.169931>

697 Shekhar A, Humphrey V, Buchmann N, Gharun M (2024b). More than three-fold increase of  
698 extreme dryness across Europe by end of 21st century. <https://doi.org/10.21203/rs.3.rs-3143908/v2> (under review in *Weather and Climate Extremes*)

700 Shekhar A, Buchmann N and Gharun M (2022) How well do recently reconstructed solar-  
701 induced fluorescence datasets model gross primary productivity? *Remote Sens. Environ.* 283,  
702 113282

703 Tripathy, K. P., & Mishra, A. K. (2023) How unusual is the 2022 European compound drought  
704 and heatwave event? *Geophysical Research Letters*, 50, e2023GL105453.  
705 <https://doi.org/10.1029/2023GL105453>

706 Tsakiris, G. and H. Vangelis, 2005. Establishing a Drought Index Incorporating  
707 Evapotraspiration. *European Water* 9/10: 3-11.

708 van der Woude, A.M., Peters, W., Joetzjer, E. *et al.* Temperature extremes of 2022 reduced  
709 carbon uptake by forests in Europe. *Nat Commun* 14, 6218 (2023).  
710 <https://doi.org/10.1038/s41467-023-41851-0>

711 van der Molen MK, Dolman AJ, Ciais P et al (2011) Drought and ecosystem carbon cycling.  
712 *Agric for Meteorol.* 151(7):765–773. <https://doi.org/10.1016/j.agrformet.2011.01.018>

713 Zhang J, Xiao J, Tong X, Zhang J, Meng P, Li J, Liu P, Yu P (2022) NIRv and SIF better estimate  
714 phenology than NDVI and EVI: Effects of spring and autumn phenology on ecosystem  
715 production of planted forests. *Agricultural and Forest Meteorology* 315, 108819

716 Zhou, S., Yu, B. and Zhang, Y. (2023). Global concurrent climate extremes exacerbated by  
717 anthropogenic climate change. *Sci. Adv.* 9(10), p.eabo1638. doi:10.1126/sciadv.abo1638.

718 Wable PS, Jha MK, Shekhar A. Comparison of drought indices in a semi-Arid River basin of  
719 India. *Water Resour Manag.* 2019;33:75–102. doi: 10.1007/s11269-018-2089-z

720 Wang B, Chen T, Xu G, Wu G, Liu G (2023) Management can mitigate drought legacy effects  
721 on the growth of a moisture-sensitive conifer tree species. *Forest Ecology and Management*  
722 544, 121196. <https://doi.org/10.1016/j.foreco.2023.121196>